Journal of Environmental Management 347 (2023) 119074

Contents lists available at ScienceDirect

Journal of Environmental Management

journal homepage: www.elsevier.com/locate/jenvman

Research article

The use of hydrodynamic cavitation for waste-to-energy approach to enhance methane production from waste activated sludge

Mojca Zupanc [a], Barbara Brajer Humar [b], Matevž Dular [a], Jurij Gostiša [a], Marko Hočevar [a], Sabina Kolbl Repinc [c,d], Mario Krzyk [c], Lovrenc Novak [a], Jernej Ortar [a], Žiga Pandur [a], Blaž Stres [c,d,e], Martin Petkovšek [a,*]

[a] Faculty of Mechanical Engineering, University of Ljubljana, Ljubljana, Slovenia
[b] JP CCN Domžale-Kamnik d.o.o., Domžale-Kamnik WWTP, Domžale, Slovenia
[c] Faculty of Civil and Geodetic Engineering, University of Ljubljana, Ljubljana, Slovenia
[d] National Institute of Chemistry, Hajdrihova Ulica 19, 1000 Ljubljana Slovenia
[e] Jozef Stefan Institute, Department of Automation, Biocybernetics and Robotics, Ljubljana, Slovenia

ARTICLE INFO

Handling Editor: Prof Raf Dewil

Keywords:
Hydrodynamic cavitation
Waste activated sludge
Disintegration
Viscosity
Methane production
Energy balance

ABSTRACT

Anaerobic digestion in wastewater treatment plants converts its unwanted end product – waste activated sludge into biogas. Even if the process is well established, pre-treatment of the sludge can further improve its efficiency. In this study, four treatment regimes for increasing methane production through prior sludge disintegration were investigated using lab-scale cavitation generator and real sludge samples. Three different cavitating (attached cavitation regime, developed cloud shedding cavitation regime and cavitation in a wake regime) and one non-cavitating regime at elevated static pressure were studied in detail for their effectiveness on physical and chemical properties of sludge samples. Volume-weighted mean diameter *D[4,3]* of sludge's particles decreased by up to 92%, specific surface area increased by up to 611%, while viscosity (at a shear rate of 3.0 s^{-1}) increased by up to 39% in the non-cavitating and decreased by up to 24% in all three cavitating regimes. Chemical changes were more pronounced in cavitating regimes, where released soluble chemical oxygen demand (sCOD) and increase of dissolved organic matter (DOM) compounds by up to 175% and 122% were achieved, respectively. Methane production increased in all four cases, with the highest increase of 70% corresponding to 312 mL CH_4 g^{-1} COD. However, this treatment was not particularly efficient in terms of energy consumption. The best energy balance was found for the regime with a biochemical methane potencial increase of 43%.

1. Introduction

The needs of the ever-growing world population generate colossal amounts of waste, resulting in alarming levels of pollution. Biological wastewater treatment plants (WWTPs), the last barrier between ever-increasing human activities and the environment, produce huge amounts - up to 13 million tonnes per year in the EU alone (Gherghel et al., 2019) - of unwanted by-product - waste activated sludge (WAS). The high cost of disposing of WAS, which currently accounts for up to 60% of the total operating costs of WWTPs (Gherghel et al., 2019; Gonzalez et al., 2018), necessitates an improvement in disposal methods. Currently, the most common methods of disposing of WAS include agricultural reuse and incineration (Gherghel et al., 2019), but each of these methods has its limitations in terms of environmental or economic issues (Lee and Han, 2013; Khanh Nguyen et al., 2021).

On the positive side, the cost of incineration can be reduced in part by reducing the amount of sludge to be disposed of, for which anaerobic digestion (AD) can be used (Nabi et al., 2019). In this process, WAS is considered as a resource rather than an undesirable end product, which is an important step towards sustainable wastewater (WW) treatment. Considering the urgent situation in which the countries of the European Union currently find themselves, with their economic and financial security threatened by the disruption of gas supplies, they need to think about how to become energy self-sufficient as soon as possible. One way is to develop technologies that can improve energy production from a source that never dries up and whose quantity is ever increasing, WAS. Bioconversion of WAS in AD simultaneously produces biogas and reduces the final volume of sludge to be disposed (Parandoush and

* Corresponding author.
E-mail address: martin.petkovsek@fs.uni-lj.si (M. Petkovšek).

https://doi.org/10.1016/j.jenvman.2023.119074
Received 16 May 2023; Received in revised form 30 June 2023; Accepted 30 August 2023
Available online 5 October 2023

Mokhtarani, 2022; Xu et al., 2020). The four crucial phases of hydrolysis, acidogenesis, acetogenesis and methanogenesis of WAS must occur sequentially at AD to produce a renewable bioenergy source - methane (Lee et al., 2019). Despite being well established, there is still room for improvement of the process as long hydraulic retention times and low hydrolysis efficiency (Xu et al., 2020; Grübel and Suschka, 2015) prevent AD from becoming an indispensable component of future WWT and making a significant contribution to meeting current and future energy needs (Lee and Han, 2013). WAS is in its essence a complex and dense mixture of microorganisms connected by a water suspension of extracellular polymeric substances (EPS), forming flocs of different sizes and compositions. The flocs contain organisms such as bacteria, protozoa, viruses, helminths, algae and fungi (Rajasulochana and Preethy, 2016), while biopolymers such as polysaccharides, proteins, humic substances, nucleic acids and lipids form the EPS (Cai et al., 2018; Mancuso et al., 2021), with proteins and polysaccharides being the most representative (Ferrentino and Andreottola, 2020; Yao et al., 2022). Since the latter and microorganisms are entrapped together in flocs, forming a complex and variable matrix, their accessibility and thus biodegradability during AD is hindered (Gonzalez et al., 2018; Ruiz-Hernando et al., 2022).

For this reason, the introduction of pre-treatment processes prior to AD seems a logical step and could help AD to finally reach its full potential. These processes accelerate and facilitate hydrolysis by breaking down the flocs and cells of the microorganisms, thereby releasing, dissolving, and degrading the trapped nutrients and particulate organics for subsequent AD (Grübel and Suschka, 2015; Mancuso et al., 2021; Zubrowska-Sudol et al., 2018; Kim et al., 2019). There are several pre-treatment options, including thermal, chemical, biological, and mechanical processes, which have been thoroughly investigated at both lab and pilot-scale (Khanh Nguyen et al., 2021; Carrère et al., 2010; Neumann et al., 2016; Zhen et al., 2017; Wang et al., 2023). Each of these processes has its advantages and disadvantages, but the most important characteristics, of which each process should have at least some, if not all, are i) suitability for industrial use, ii) effectiveness, iii) efficiency, iv) ease of integration and maintenance, v) ability to be upgraded, vi) ability to easily change operating conditions, and vii) ability to be coupled with other processes to enhance the desired effect. One of the promising mechanical pre-treatment approaches that meets many of these requirements is the phenomenon of cavitation, in which a sudden drop in pressure triggers the formation of vapour and gas bubbles in a liquid medium. Hydrodynamic cavitation (HC) is gaining attention as an effective, easily scalable, and efficient method for treating WAS. The various investigated HC designs can be broadly divided into static (throttling) and dynamic devices. The former include orifice plates (Lee and Han, 2013; Lee et al., 2019; Cai et al., 2018), (Şağban et al., 2018), Venturi tubes (Grübel and Suschka, 2015; Kim et al., 2008), swirling jet-induced HC (Mancuso et al., 2017, 2019; Ferrentino and Andreottola, 2020), and high-pressure homogenizers (Fang et al., 2015). The latter include rotating generators of hydrodynamic cavitation (RGHC) (Bhat and Gogate, 2021; Patil et al., 2016) and high-speed homogenizers (Lee et al., 2019; Zhang et al., 2012). Common to all dynamic devices are high shear stresses, which play an important role in breaking up WAS flocs. RGHCs have certain advantages over other HC devices, which has driven the development of novel designs in recent years, such as serrated discs (Petkovšek et al., 2015; Vilarroig et al., 2020), dimpled rotors (Kim et al., 2019; Patil et al., 2016; Zubrowska-Sudol et al., 2020) and pinned discs (Gostiša et al., 2021; Kolbl-Repinc et al., 2022). However, in the design of HC devices, special attention still needs to be paid to cavitation erosion and wear of the cavitating parts. Design and development can be done by either experimental or numerical modelling (Gostiša et al., 2022, 2023; Hou et al., 2023; Mancuso, 2018) which is usually faster and economically more feasible, but needs to be validated.

The objective of this study was to investigate how four different treatment regimes affect WAS disintegration and subsequent methane production in three rotor-stator geometry configurations of lab-scale RGHC device. The treatment regimes differed in the extent and type of cavitation - from A) no cavitation to B) attached cavitation, C) fully developed cloud shedding cavitation, and D) cavitation in the wake. The effects of all regimes were compared based on 1.) characterization of developed conditions in tap water (TW), 2.) analysis of the physical and chemical properties of WAS, and 3.) energy balance. Even though RGHC devices have many of the features mentioned above, the technology is still far from its peak. The gap between understanding and exploiting specific cavitation conditions is significant, so further, more detailed studies are needed to unlock the full potential of HC. It is becoming increasingly clear that the nature of cavitation and its specific hydrodynamic effects strongly influence the properties of WAS and thus the effectiveness and efficiency of AD. Lab-scale studies are best suited for this task because they are easier to conduct, and more experiments can be performed in less time. This is the only way to capture the full potential of the technology and accelerate the transfer of knowledge to pilot and industrial scale.

Table 1
Characteristics of WAS and anaerobic inoculum collected for the purpose of the present experiments.

Parameter	Waste activated sludge (WAS)	Anaerobic inoculum
pH	6.8 ± 0.1	7.3 ± 0.1
Redox potential (mV)	26.6 ± 0.3	4.0 ± 0.3
TS (g L^{-1})	17.9 ± 0.5	28.1 ± 0.9
VS (g L^{-1})	13.1 ± 0.5	10.0 ± 0.1
tCOD (g L^{-1})	9.4 ± 2.9	16.4 ± 0.1
sCOD (mg L^{-1})	272 ± 0	–
TN (mg L^{-1})	1075 ± 5	1435 ± 15
NH_4–N (mg L^{-1})	16 ± 0	926 ± 36

TS: total solids; VS: volatile solids; tCOD: total chemical oxygen demand, TN: total nitrogen; NH_4–N: ammonium.

2. Materials and methods

2.1. WAS and anaerobic inoculum collection and their characteristics

WAS samples used for the experiments represent a surplus secondary WAS from the SBR (sequencing batch reactor) basins of a local WWTP treating municipal and industrial WW with a capacity of 149,000 PE. WAS sample containing 1.8% TS was taken from the secondary settling tank. Along with WAS, a sample of anaerobic inoculum (characteristics listed in Table 1) was also collected from the operating anaerobic digester at the same WWTP and used as inoculum for biochemical methane potential (BMP) analysis. WAS samples were used in the period of 1 h after collection to prevent any decomposition.

2.2. Experimental set-up

The experimental setup (Fig. 1) consists of the RGHC (1) driven by a 1.5 kW electric motor (2) and a 7 L reservoir (3) connected to a closed circuit, with all parts made of stainless steel. On the pressure side, the flow rate was measured with an electromagnetic flow meter ABB ProcessMaster 610 (a), while the inlet and outlet pressures of the RGHC were measured with an ABB 2600 T absolute (b) and differential (c) pressure transducer, respectively. To maintain a constant temperature of the treated sample, a cooling coil (4) was installed in the reservoir and connected to the DuraChill external portable cooling unit with a cooling capacity of 1.28 kW. The temperature was monitored using a 4-wire RTD Pt100 thermometer (Class A) (d) installed directly in the reservoir. An outlet valve (5) allows samples to be released for analysis during treatment and at the end of each experiment. Characterization of cavitation was assessed by high-speed photography using the Photron SA -Z camera (e) at 51,200 fps and 450 × 120 pixel resolution. Pressure fluctuations were measured using a high-frequency pressure sensor (f), PCB Piezotronics 133B28, with a sampling frequency of 500 kHz via a

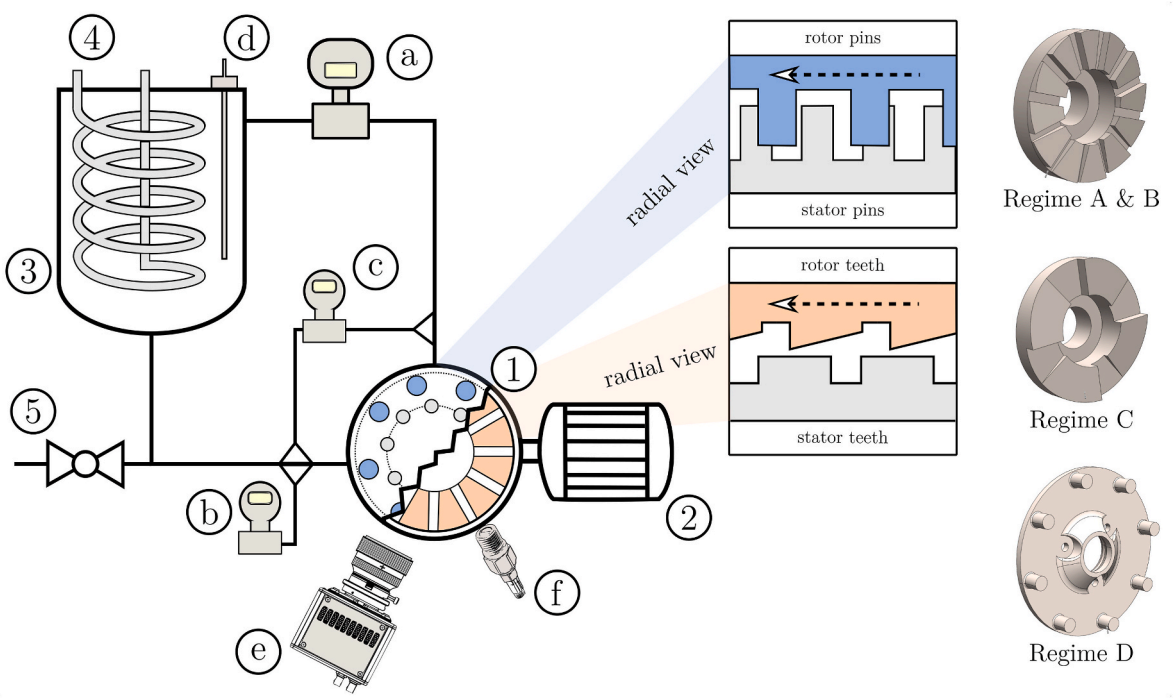

Fig. 1. Lab-scale RGHC scheme: (1) cavitation chamber, (2) electrical motor, (3) reservoir, (4) cooling coil and (5) outlet valve. Measurement equipment: (a) electromagnetic flow meter, (b) absolute pressure transducer, (c) differential pressure transducer, (d) thermometer, (e) high-speed camera and (f) high-frequency pressure sensor. SD version of RGHC is colored orange while PD version is colored blue.

National Instruments measurement card NI-9222.

2.2.1. Rotating generator of HC

The RGHC experimental unit was developed and constructed at the Faculty of Mechanical Engineering, University of Ljubljana. Its major advantage over other rotating cavitation devices is its dual function: cavitation generation and pumping performance. It operates as a rotor-stator cavitation generator with axial inlet and radial outlet and uses centrifugal forces for pumping. Three different rotor-stator geometry configurations were used in this study: i) serrated 12 teeth rotor with 10 teeth stator, ii) serrated 4 teeth rotor with 10 teeth stator and iii) a rotor with 8 and a stator with 15 cylindrical pins. Part of the housing with stators were made out of transparent acrylic glass in order to enable visualization of cavitation phenomena.

Serrated rotor-stator configuration, referred to as serrated disc (SD) RGHC consists of a toothed rotor-stator combination. The outer diameter of the 12-tooth and 4-tooth rotors was 50 mm, with each tooth having an inclination of 10.7°. The stator in both cases had the same diameter of 126 mm and 10 grooves with a width of 3 mm and a depth of 2 mm, resulting in flat stator teeth. The main feature of SD RGHC is that the rotor tooth passing the stator tooth resembles a venturi constriction during operation, creating periodically recurring pressure oscillations. A detailed description of the principle of operation of SD RGHC was previously described in (Petkovšek et al., 2015; Stepišnik Perdih et al., 2017). The RGHC configuration with pinned disc (PD) consists of a rotor with 8 pins with a diameter of 6.5 mm and 8 mm high, equidistantly placed 35 mm from the centre of the disc with diameter of 78 mm. The stator disc consists of 15 pins with a diameter of 5 mm and 8 mm in height arranged at a distance of 27.5 mm from the centre.

Visualization and pressure fluctuation measurements were performed on tap water (TW) samples because visualization in WAS samples is not possible due to turbidity. We are aware that there are differences between conditions developed in TP or WAS samples, however variations between the regimes were expected to be in the same range for both liquids. Energy consumption during the four selected regimes was measured directly in the samples using the Power Analyzer - Norma 4000. To determine the amount of energy transferred from the rotor-stator to the WAS samples (Table 6), additional measurements of energy losses between the electric motor, bearings, seals, and rotor in air were made.

2.3. Experimental conditions and design

Four different treatment regimes (A – non-cavitating; B, C, D – cavitating) were selected for three different rotor-stator configurations described previously (Table 2). The selection was focused on finding the optimal treatment regime to achieve the highest subsequent CH_4 production. Regime A included SD RGHC with a 12-tooth rotor configuration at elevated static pressure in the test rig (6 bar absolute pressure) to suppress cavitation formation and isolate only shear on macro scale. Regime B with SD RGHC and a 12-tooth rotor generates attached cavitation at each tooth. Regime C with 4 teeth SD RGHC favours the

Table 2
Experimental conditions for the 4 investigated regimes. Experiments A, B and C were performed on SD RGHC while experiment D was performed on PD RGHC.

Regime	N_r	N_s	n (rpm)	V (L)	Time (min)	Np	T (°C)	p_0 (kPa)	Δp (kPa)	Q (L min^{-1})
–	initial, non-treated									
A	12	10	10,800	5	15	60	26 ± 2	598.6	25.6	20
B								−1.3	24.3	
C	4							−1.6	35.0	
D	8	15	7000		12			−4.2	172.9	25

generation of cloud shedding cavitation. Regime D with the PD RGHC configuration results cavitation forming in wake behind the cylindrical shapes - the pins. The 4 treatments were compared based on the same number of cavitation passes (Np=(Q•t)/V), where Q is the volumetric flow rate of the sample, t is the time of cavitation, and V is the sample volume. Number of Np were selected to assure potential differences between the regimes to occur. To ensure approx. the same circumferential velocity – 28 m s^{-1} of the rotors at different diameters (SD - 50 mm and PD -78 mm), the rotational frequency was set to 10,800 rpm in the case of SD and 7000 rpm in the case of PD. Power P and energy E are given after subtracting the additional losses measured. The experimental conditions and the parameters measured during the experiments are listed in Table 2.

N_r: number of rotor teeth/pins; N_s: number of stator teeth/pins, Np: number of cavitation passes, p_0: gage pressure at RGHC inlet.

2.4. Sample preparation and analyses

Experiments were performed within 1.5 h of WAS sampling. 50 L of the sample was poured into a container and mixed vigorously to obtain the same initial samples for all 4 planned experiments. 5 L of the well mixed WAS sample was used for each experiment. Appropriate amounts of samples were collected for analyses before the experiments and after 60 Np. All analyses were performed in triplicate. The effectiveness and efficiency of the 4 treatment regimes studied were compared by analysing the physical and chemical properties of WAS, BMP analysis, and calculation of energy balance.

2.4.1. Analytical methods for evaluation of WAS samples

Before and after each treatment, WAS samples were evaluated by analysing their physical and chemical properties. Physical properties were evaluated by particle size and distribution, microscopic analysis, and viscosity measurements, while chemical properties were evaluated by analysis of released organic and inorganic soluble compounds. Detailed descriptions of most of the analyses performed as part of this study are described in detail elsewhere (Kolbl-Repinc et al., 2022).

Particle size and distribution analysis. For particle size and distribution of WAS samples particle sizer analyzer Analysette 22 MicroTec Laser Particle sizer - Wet Dispersion Unit (Fritsch, Germany) following ISO 13320 - Laser Diffraction Methods was used (Kolbl-Repinc et al., 2022). Percentile results are presented as d10, d50 and d90, while volume-weighted mean diameter, also known as De Brouckere mean diameter, is presented as *D[4,3]*.

Microscopic analysis. In addition to the Nikon Eclipse 80i used previously, differential interference contrast (DIC) microscopic images of WAS samples were also acquired using a Zeiss Axio Observer Z1 microscope at magnifications of 100×, 200x, 400x, and 1000x. 10 μl of sample was placed on a microscopic glass slide, covered with a #1.5 cover glass (22 × 22 mm) and viewed under the microscope.

Viscosity measurements. Rheological measurements of the WAS samples were performed with a rotary rheometer (Anton Paar Physica MCR302) using a parallel plate 25 mm (PP25) measuring system with 1 mm measuring gap. Approximately 500 μl of the sample was pipetted onto the bottom of the rheometer plate prior to measurements. Viscosity was measured at shear rates from 3 to 200 s^{-1} in 25 logarithmically distributed steps and complex viscosity was determined with a frequency sweep measurement at a shear strain of 0.1% with an angular frequency of 0.1–250 rad s^{-1} in 25 logarithmic steps. The consistency index indicates the average firmness of the sample, while the flow index *n* is a dimensionless index of flow behavior and is equal to 1 for Newtonian fluids, greater than 1 for dilatant fluids, and less than 1 for pseudoplastic fluids (Zhang et al., 2019; Hong et al., 2018). The Herschel-Bulkley model (Eshtiaghi et al., 2013) was used to fit the rheological data, as shown in equation (1):

$$\tau = \tau_y + k \bullet \dot{\gamma}^n \quad (1)$$

where τ_y is yield stress (Pa), $\dot{\gamma}$ is the shear rate (s^{-1}), *n* in the flow index and *k* is the consistency index ($Pa \bullet s^n$). The Ostwald-de Waele model was used to fit the experimental viscosities η_e by equation (2) (Ruiz--Hernando et al., 2022):

$$\eta_e = K\dot{\gamma}^{n-1} \quad (2)$$

where $\dot{\gamma}$ is the shear rate (s^{-1}), *n* is the power law index (−) and *k* is the consistency index ($Pa \bullet s^n$).

Analyses of released organic and inorganic compounds Measurements of pH, redox potential, and temperature were made before and after treatment (Supplementary Material, Suppl. 1). Soluble chemical oxygen demand (sCOD), total nitrogen (TN), and nitrogen species NH_4–N and NO_3–N were prepared and measured in the same manner as described in (Kolbl-Repinc et al., 2022). Total solids (TS), volatile solids (VS), total COD (tCOD), and total suspended solids (TSS) were determined according to APHA Standard Methods (*APHA (2005)* Standard Methods for the Examination of Water and Wastewater. 21st Edition, American Public Health Association/American Water Works Association/Water Environment Federation, Washington DC., 2005). The disintegration degree (DD) was calculated according to the equation given in Suppl. 2 (Kolbl-Repinc et al., 2022). To determine the maximum chemical disintegration ($sCOD_{max}$), 1 M NaOH (Sigma-Aldrich, Germany) was added to the initial sample at a ratio of 1:2 and heated at 90 °C for 10 min. The value of $sCOD_{max}$ was 2406 ± 78 mg L^{-1}.

Dissolved organic matter (DOM) was characterized by spectrophotometric measurements (Helms et al., 2009; Twardowski et al., 2004) and 3D excitation-emission (Ex-Em) spectral profiles (Helms et al., 2009). A detailed description of all spectral analyses can be found in Suppl. 4. Chromogenic DOM was characterized by calculating molecular weight (MW) indices: specific ultraviolet absorbance (SUVA245), E465/E665 ratio, and sum of absorbances (A250-A450). Characteristic wavelengths were extracted for nucleic acid characterization (A260, A320). Finally, DNA purity index A260/320 was calculated to determine the extent of change in the contribution of compounds other than DNA (PROMEGA application note, ("PROMEGA Application Note [WWW Document], n.d. URL https://worldwide.promega.com/resources/pubhub/enotes/how-do-i-determine-the-concentration-yield-and-purity-of-a-dna-sample/(accessed 11.17.22, page 1).)).

2.4.2. Biochemical methane potential (BMP) analysis

The automated methane potential Test System (AMPTS II, Bioprocess Control) for accurate and rapid on-line measurements of ultra-low biomethane flows was used to measure the BMP of WAS samples after treatment. 15 anaerobic reactors with a volume of 0.5 L were used and heated to a temperature of 37 °C in a water bath throughout the experiment. Mixing of the anaerobic reactors was achieved by computer-controlled mechanical stirrers with 5 min of mixing and 30 min of pause. A 3 M NaOH solution was used for CO_2 fixation (Kolbl et al., 2014).

First the 500 mL glass reactors were filled with 400 mL of anaerobic inoculum from the operating anaerobic digester of the local WWTP. Then, 33.4 mL of non-treated and treated WAS samples were used as substrates and added to the reactors. Positive controls with glucose (3.4 g) and negative controls without glucose (anaerobic inoculum only) were used to evaluate the quality of the inoculum. For each sample, the reactors were run in parallel. Before the start, the reactors were flushed with N_2 for 2 min to ensure anaerobic conditions in the reactors. At the end of the experiment, the methane produced in the reactors containing only inoculum was subtracted from the amount of methane produced in the other reactors as described previously (Kolbl et al., 2014, 2017).

2.4.3. Energy balance calculations

The energy balance of the 4 selected regimes (Table 2) was compared by calculating 6 specific parameters (Table 6). The power required for treatment (P_{tre}) was calculated directly from energy consumption

measurements, subtracting losses between the electric motor, bearings, seals, and rotor. The specific energy of sludge solubilization (SESS, kJ g^{-1} sCOD) was calculated according to (Mancuso et al., 2017; Kolbl-Repinc et al., 2022; Garlicka and Zubrowska-Sudol, 2020). The difference in the amount of CH_4 produced after 42 days between treated and non-treated WAS samples was calculated using tCOD (see Results 3.4). For energy balance calculations, the potential amounts of CH_4 produced by 5 L of the WAS samples were used ($CH_4$5L). The energy extracted from CH_4 (EE_g) was calculated using the calorific value of CH_4 of 36.2 kJ L^{-1} (891 kJ mol^{-1}; 24.6 L mol^{-1} at 300 K for ideal gas), while the energy required to operate the RGHC (EE_r) was determined as P_{tre}•t. EE_g-EE_r represents the energy balance, the difference between produced and consumed energy.

2.4.4. Statistical analysis

Statistical analysis was conducted using the JMP Pro 16 software. Pearson's correlation coefficient (R) was used to evaluate the linear relationship between two different parameters (variables). To compare the effect of the selected treatments oneway ANOVA and paired Student's t-test were performed. Oneway ANOVA was used to test the differences in the means of different treatment regime and Student's t-test was used to test pairwise differences in means of treated WAS samples (JMP Learning Library, ("Jpm learning library," n.d.)). Detailed statistical analyses are given in Suppl. 3 and 5.

3. Results and discussion

3.1. Visualization and pressure analysis of treatment regimes

Cavitation characterization was performed through high-speed imaging and pressure analysis for 4 treatment regimes. Fig. 2 – left compares 4 selected treatment regimes, where the upper part of the figure is a schematic representation of cavitation on the rotors, while the lower part shows an image sequence with 0.2 ms time steps. Evaluation of these regimes with high-speed photography and high-frequency pressure pulsations highlights the main features and differences between the selected regimes. Rotors in all regimes rotate counterclockwise. Selected teeth (regimes A, B, C) and pins (regime D) are outlined in orange and blue, respectively. In regime A, static pressure was increased (Table 2) to eliminate cavitation formation and isolate shear on macro scale only. In other three selected regimes shear on macro and micro scale, due to presence of collapsing cavitation bubbles, was present. In regime B, cavitation formed behind the leading edge of each rotor tooth. Due to the relatively short spatial and temporal conditions, the high-pressure region of the next tooth reaches the cavitation at the previous tooth, so it cannot develop in the form of shedding clouds as in regime C. In regime C, where only four teeth are arranged across the rotor, cavitation has sufficient space and time to grow from the leading edge to a greater extent with shedding parts toward the trailing edge of the rotor tooth. In regime D, a cavitation in a wake formed behind each rotor pin, creating a short but distinct von Karman vortex street.

At this point, it is important to emphasise that in the presented RGHC setup, shear must be considered at two scale levels: i) at the macro scale - movement of the rotor in the vicinity of the stator, and ii) at the micro scale - formation and collapse of cavitation structures. In order to exclude the presence of cavitation (regime A) at the same rotation frequency of the rotor, it is necessary to provide a high static pressure, which might also affect the shear on macro scale and consequently WAS characteristics. In this way, the characteristics of high-speed and high-pressure homogenizers (Lee et al., 2019; Fang et al., 2015) are mimicked. Similarly, but not in the same way, others have attempted to study the effects of cavitation and shear on macro scale alone (Yao et al., 2022; Kim et al., 2020). They simply overcame cavitation formation at the orifice with a bypass (Yao et al., 2022) or changed the geometry of their rotor-stator cavitation device (Kim et al., 2020). In the latter the effect of circulation pumps on WAS disintegration was neither mentioned nor considered.

The correlations between the measurements of the pressure pulsations (Fig. 2 – right) and the visualization (Fig. 2 – left) fit well. In the non-cavitating regime A the standard deviation (STD) of the pressure pulsation is the lowest, while it gradually increases from regime B to C, where it peaks. In regime D, the STD is slightly lower than in regime C. Measured pressure pulsations and calculated STDs (Fig. 2 – right) can indicate presence of cavitation and its intensity to some extent but cannot be exclusively used for detailed cavitation characterization. Since the high-frequency pressure transducer can most likely only detect macro-scale phenomena, such as the passing of a tooth or a pin near the stator geometries or the collapse of the cavitation cloud, all of which produce a strong pressure wave, micro-scale phenomena such as the collapse of individual cavitation bubbles may be distorted and go unnoticed.

3.2. WAS physical properties evaluation before and after treatment

Particle size and distribution. The effects of the 4 selected regimes (Table 2–A, B, C, and D) on floc and particle disintegration were studied by measuring particle size and distribution. All 4 regimes had a strong effect and resulted in a significant decrease in mean particle size *D[4,3]* from 128.2 to 10.4 μm after treatment (Table 3). There was statistically significant strong linear correlation (positive or negative) between mean particle size *D[4,3]*, d10, d50, d99, mode and specific surface area

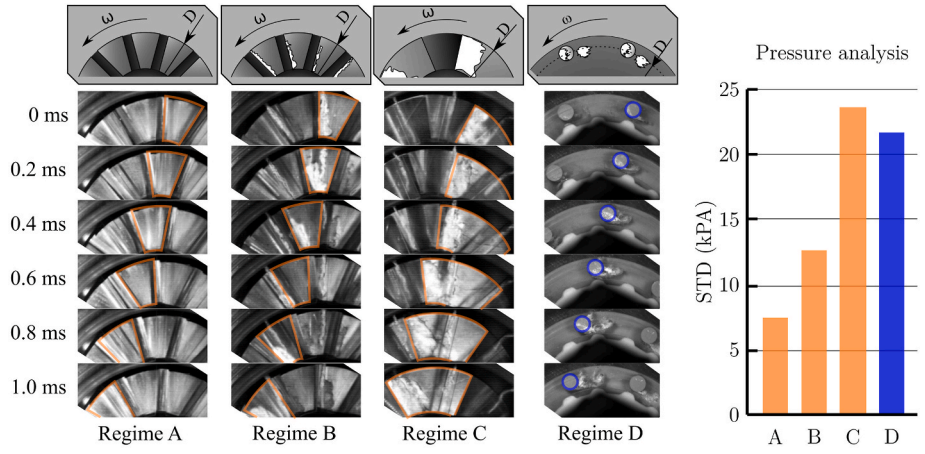

Fig. 2. Visualization (left) and pressure analysis (right) of the 4 selected regimes with schematic presentation of cavitation presence. Regime A – no cavitation, regime B – attached cavitation, regime C – developed cloud shedding cavitation, regime D – cavitation in a wake.

Table 3
Particle size and distribution before (0) and after treatments (sample A – no cavitation regime, B – attached cavitation regime, C - developed cloud shedding cavitation regime and D – cavitation in a wake regime).

Sample	0	A	B	C	D
D[4,3] (μm)	128.2 ± 7.6	10.4 ± 0.2	11.5 ± 0.4	10.6 ± 0.3	13.7 ± 1.4
mode (μm)	157.1 ± 22.0	10.9 ± 0.2	12.2 ± 0.5	11.1 ± 0.8	11.1 ± 0.5
d10 (μm) [%]	19.5 ± 3.4	3.5 ± 0.1	3.6 ± 0.1	3.4 ± 0.1	3.9 ± 0.1
d50 (μm) [%]	112.2 ± 9.7	9.3 ± 0.1	10.3 ± 0.3	9.5 ± 0.3	10 ± 0.6
d90 (μm) [%]	256.2 ± 10.2	18.6 ± 0.3	20.8 ± 0.8	19.5 ± 0.7	25.7 ± 2.0
specific surface area (cm^2/cm^3)	1.8 ± 0.2 × 10^6	10.6 ± 0.3 × 10^6	10.2 ± 0.2 × 10^6	11.0 ± 0.2 × 10^6	10.1 ± 0.4 × 10^6
span	2.1 ± 0.1	1.6 ± 0.0	1.7 ± 0.0	1.7 ± 0.1	2.2 ± 0.2

(Suppl. 3). There was no significant difference in mean particle size *D[4,3]* between samples A, B and C, but a significant difference was found between these three samples and sample D (Suppl. 5). The difference came from a minor secondary peak in sample D at around 70 μm (Suppl. 6), which could be due to re-flocculation as described in (Pilli et al., 2011). The smallest mean particle size *D[4,3]* and span were obtained for regime A, in which only shear on macro scale occurred. In this case, the distribution width (d10 to d90) was also most effectively reduced from the initial range of 19.5–256.2 μm to a range of 3.5–18.6 μm. D10, d50, and d90 of all treated samples decreased significantly (82.6–92.7%), indicating that WAS particles of all sizes were sensitive to treatment. The increased number of particles smaller than 1 μm (Suppl. 6) also correlated with the decrease in TSS concentration of treated samples (Table 5 and Suppl. 3). A significant statistical difference in specific surface area was observed between treated samples C–D, C–B, A-D, and A-B (Suppl. 5). The reduction in particle size and increase in specific surface area are important because they improve the contact between substrate, enzymes and anaerobic bacteria, which translates into improved biogas production (Mancuso et al., 2021; Kim et al., 2019; Garuti et al., 2018).

Based on HC regimes B, C, and D, the results of particle size and distribution can be correlated with the extent of cavitation and the intensity of pressure pulsation (Fig. 2). The results in regime C gave the smallest mean particle size *D[4,3]* values and consequently the highest specific surface area. This indicates that the extent and intensity of cavitation play an important role and that the cavitation properties must be carefully selected to achieve the desired effects. Since regimes A and C resulted in almost the same particle size and distribution, one could even argue that the presence of cavitation is not beneficial and that only shear on macro scale is responsible for the reduction in particle size. As discussed in Section 3.1, shear occurs at both the macro and micro scale, implying that shear on macro scale could be sufficient to reduce particle size in our case. A similar reduction in mean particle size has been reported in other studies using an orifice design (Cai et al., 2018; Yao et al., 2022) or rotating HC devices (Kim et al., 2019; Kolbl-Repinc et al., 2022). In contrast to our results, Yao et al. and Kim et al. reported significantly better results when both shear on macro scale and cavitation were present (Yao et al., 2022; Kim et al., 2020). They suggested that shear on macro scale alone can only affect WAS flocs, while in combination with cavitation it can additionally destroy the cell structures of microorganisms present in WAS due to stronger shear forces, higher velocity, turbulence and partial pressure fluctuations (Yao et al., 2022; Kim et al., 2020). In our case, shear on macro scale developed in regime A proved to be as effective in breaking up the flocs as shear on macro scale combined with shear on micro scale due cavitation (regimes B, C and D). The observed differences between the studies could be due to the fact that the shear on macro scale developed in the orifice design was not sufficient to seriously damage the flocs (Yao et al., 2022), while the efficiency in the rotating device was lower (Kim et al., 2020) compared to our study. A detailed comparison between our results and those of Kim et al. (2020) is not possible due to lack of details on the geometry of the rotor, which prevents the calculation of the circumferential velocity of the rotor, which is strongly related to the shear rate. Comparing the 4 regimes studied, we have shown that chemical effects, namely the formation of $^{\bullet}OH$ due to the collapse of cavitation bubbles, do not contribute to the disintegration of WAS and that mechanical effects must be primarily responsible. The same conclusion was drawn by Zhen et al. (2017) for AC.

Microscopic analysis. The microscopic images of non-treated (sample 0) and treated samples (A, B, C and D) showed a rich community of microorganisms with the presence of common WAS representatives such as ciliates, rotifiers, nematodes, filamentous bacteria, spirochetes, fungi and algae, etc. (Suppl. 7). Most of the observed microbial communities were viable and motile, with a small proportion of damaged populations. All treatments visibly reduced the size of the flocs, which is consistent with the particle size measurements mentioned above and available literature (Cai et al., 2018; Petkovšek et al., 2015). In addition, increased numbers of damaged microbial populations were observed, e.g., damaged ciliates (e.g., *Epistilys* body separated from the stalk – Suppl. 7b), reduced length of filamentous bacteria (Suppl. 7c), spirochetes were hardly observed. We can assume that when the treatments damage the cell walls, they could also lead to the destruction of biopolymers on the surface of the cells, affecting the composition of the final sample and consequently the formation of methane.

Viscosity measurements. The rheological properties of WAS play an important role in the performance of AD. To better understand the effects of selected treatments on the rheological properties of WAS, the viscosity of non-treated and treated WAS samples was studied at different shear rates. The viscosity decreased with increasing shear rate (from 3.0 s^{-1} to 200.0 s^{-1}) for all samples. The evolution of viscosity as a function of shear rate of the non-treated sample decreased from 183.6 ± 29.6 to 17.0 ± 0.7 mPa s with an increase in shear rate from 3.0 to 200.0 s^{-1} (Suppl. 8a). There were significant differences in viscosity between the treated sample A and samples 0, B, C and D (Suppl. 5), demonstrating the effect of different treatment regimes. The increase in viscosity was observed for sample A over the entire shear rate range, while the viscosity of samples B, C, and D decreased from 254.8 ± 28.4 mPa s to 157.7 ± 27.4, 145.0 ± 19, and 138.7 ± 0.6 mPa s, respectively, at the

Table 4
Fitting results of the Herschel-Bulkley and Ostwald-de Waele model and the key parameters of non-treated (0) and treated samples (sample A – no cavitation regime, B – attached cavitation regime, C - developed cloud shedding cavitation regime and D – cavitation in a wake regime).

Sample	Consistency index (Herschel-Bulkley parameters)			
	$k\ (Pa \bullet s^n)$	n	Equation	R^2
0	0.32346	0.44112	$\tau = 0.323458 \bullet \dot{\gamma}^{0.44112}$	0.9771
A	0.56292	0.36860	$\tau = 0.56292 \bullet \dot{\gamma}^{0.3686}$	0.9952
B	0.39287	0.43351	$\tau = 0.39287 \bullet \dot{\gamma}^{0.43351}$	0.9765
C	0.33861	0.45829	$\tau = 0.338613 \bullet \dot{\gamma}^{0.45829}$	0.9785
D	0.35730	0.42614	$\tau = 0.357298 \bullet \dot{\gamma}^{0.42614}$	0.9707
	Viscosity (Ostwald-de Waele parameters)			
	$K\ (mPa \bullet s^n)$	n	Equation	R^2
0	229.152	0.54843	$\eta_e = 229.152 \bullet \dot{\gamma}^{0.54843-1}$	0.83631
A	346.117	0.72131	$\eta_e = 346.117 \bullet \dot{\gamma}^{0.72131-1}$	0.84737
B	226.223	0.60326	$\eta_e = 226.223 \bullet \dot{\gamma}^{0.60326-1}$	0.94592
C	194.087	0.62606	$\eta_e = 194.087 \bullet \dot{\gamma}^{0.62606-1}$	0.92034
D	199.748	0.60668	$\eta_e = 199.748 \bullet \dot{\gamma}^{0.60668-1}$	0.94346

shear rate 3.0 s^{-1}, but remained above the viscosity of the initial sample in the shear rate range between 17.3 and 200.0 s^{-1} (Suppl. 8a). Oneway ANOVA analysis showed that there were statistically significant differences in the viscosities between different treatment regimes, further supported by Student's *t*-test where statistically significant differences between samples A-D, A-C and A-B were determined (Suppl. 5). The viscosities of all four treated samples did not differ significantly from each other at the shear rate range above 20.6 s^{-1}, while they differed greatly below 20.6 s^{-1} (especially sample A). The detailed data on the measured viscosities and curves can be found in Suppl. 8b.

The rheological behavior of the WAS samples was studied at a steady shear flow in the range of 3.0–200.0 s^{-1} and first analyzed using the Herschel-Bulkley equation. Table 4 shows that the *k* value increased substantially only for sample A (from 0.32346 to 0.56292), while the increase was smaller for all other treated samples (up to 0.39287). Furthermore, the viscosities were fitted to the Ostwald-de Waele equation. The higher the value of *K*, the higher the viscosity, which was shown for sample A. The power index *n* increased for all treated samples, with the highest value obtained for sample A, indicating that the pseudo-plasticity decreased for the treated samples. This is consistent with the decrease in particle size, as the mean particle size *D[4,3]* decreased for the treated samples. Smaller particles are not only less pseudo-plastic than larger particles, but also less deformable (Ruiz-Hernando et al., 2014).

In other studies, opposite results were obtained. Some observed a decrease (Ruiz-Hernando et al., 2014, 2022; Kim et al., 2008; Pham et al., 2009) and others an increase (Cai et al., 2018) in viscosity, at values comparable to our study. A decrease was connected to the structural changes of WAS after treatment, whereas an increase was attributed to the release of EPS from the flocs (Cai et al., 2018). An increase was reported also by (Fang et al., 2015) who used high pressure homogenisation. We assume that in our case, the increased viscosity of sample A could be due to two reasons: i) decrease in particle size, a consequence of shear on macro scale, which are more likely to absorb moisture (Yao et al., 2022) and thus affect viscosity, and ii) release of EPS from flocs due to shear on macro scale and high pressure. Both could individually or in combination lead to stronger interparticle interactions. The reason why the decreased particle size did not affect viscosity in regimes B, C, and D could be due to the different chemical composition of these samples. In these three regimes, in addition to shear on macro scale, also shear on micro scale was present, causing disruption of the cell walls of the individual microorganisms and cleaving the bonds of the released macromolecules, thereby increasing solubilization and decreasing viscosity (Kim et al., 2019). The chemical effects induced by the collapse of the cavitation bubbles additionally trigger oxidation reactions, which lead to chemical changes in the released compounds and attenuate the effects caused by the reduction in particle size.

3.3. WAS chemical properties evaluation before and after treatment

Organic and inorganic compounds. The effects of the 4 selected regimes on WAS disintegration and solubilization were determined by evaluating the main chemical parameters. It can be concluded that all 4 treatments improved solubilization, which is due to the release of compounds from the inner part of the flocs and the cells of the individual microorganisms and the disintegration of smaller particles. However, differences were observed between the regimes (Table 5) and differences in sCOD were determined between all samples except B and D (Suppl. 5). Linear Pearson correlations confirmed the positive or negative correlations between physical (mean particle size *D[4,3]*, d10 to d99, mode, surface area) and chemical changes (sCOD) (Suppl. 3). Higher concentrations of sCOD and NH_4–N, and were always determined in regimes B, C, and D than in regime A, and regimes B and D were found to be more effective than C for the release of sCOD and NH_4–N. The same was observed for DD. The decrease in TSS, which represents the number of suspended particles observed for all 4 regimes, is consistent with the decrease in mean particle size *D[4,3]* and the increase in sCOD. The observed results indicate that the presence of shear on macro and micro scale is necessary to achieve the highest increase in soluble fractions. Although only shear on macro scale (regime A) was sufficient to reduce mean particle size *D[4,3]* (Table 3), this is not true for the degree of solubilization (Table 5). We assume that shear on macro scale alone only leads to the disintegration of flocs and larger particles and possibly some intra- and intermolecular bonds of EPS (Wang et al., 2021; Holkar et al., 2019), but is not effective enough to destroy single cells, which is why the lowest sCOD was observed for regime A (Table 5). Thermal, mechanical, and chemical effects are required to destroy them, and these are present to varying degrees in cavitating regimes B, C, and D, individually or in combination. Small areas of extremely high temperatures – local hot spots – can thermally degrade and destroy the cell walls of microorganisms in samples from WAS [54]. Mechanical effects produce high intensity shock waves, shear on micro scale and microjets in the fluid surrounding the bubbles, which can damage the cells of individual microorganisms and release their intracellular matter. These two effects lead to a higher degree of solubilization and DD, which is observed in these 3 regimes. Moreover, the collapse of cavitation bubbles also causes chemical effects, namely the formation of reactive oxygen species, which, as discussed in detail in (Zupanc et al., 2019), additionally contribute to the destruction of the cells of the microorganisms and can oxidize the released inter- and intracellular compounds in the samples. These results are consistent with the observations of (Yao et al., 2022; Kim et al., 2020). The differences in the determined sCOD values between regimes B, C and D show that relying only on the presence of cavitation and pressure pulsation measurements (Fig. 2) to draw conclusions is not always sufficient. Based on the determined STDs, which are connected to the cavitation aggressiveness, one might hastily conclude that cavitating regime C would result in the highest sCOD values, which was not the case, as regimes B and D proved superior in this regard. This suggests that cavitation phenomena may play a more important role at the micro scale (Section 3.1). Based on the visualization (Fig. 2 – left), regimes B and D appear to have a higher number of smaller cavitation bubbles, which increases the probability of a single bubble hitting a single cell. This would increase the likelihood of individual bubbles collapsing to destroy cells and increase the degree of solubilization.

Studies investigating cavitation as a pre-treatment method of WAS always result in increased solubilization (Ferrentino and Andreottola, 2020; Yao et al., 2022; Mancuso et al., 2017), but due to the different characteristics of the initial WAS, it is very difficult to directly compare the efficacy as discussed in (Kolbl-Repinc et al., 2022).

Dissolved organic matter. To determine the changes of DOM caused by the treatments, UV-VIS and Ex-Em spectral analysis before and after treatments were performed. The results show that all 4 treatments affected the samples, as UV-VIS (Table 5) and Ex-Em (Fig. 3) spectra changed. Linear Pearson correlations confirmed the statistically significant positive or negative correlations between the physical (mean particle size *D[4,3]*, d10 to d99, mode, span, surface area) and chemical changes (A260, A320, A300, sum A250-450 and E465/E665) (Suppl. 3). Increased MW of molecules (Table 5–A254) after treatments, can be attributed to newly released compounds from flocs and individual cells. In contrast to regime A, cavitating regimes also affected the aromaticity (Table 5 – SUVA), decrease of which could be because of chemical modifications of the released or already present molecules in the treated samples due to the cavitation phenomena effects. Chemical modifications were additionally confirmed by Ex-Em spectroscopy (Fig. 3), where increased fluorescence was observed in all cavitating regimes. Higher fluorescence signals determined for regimes B, C and D compared to regime A showcase the disintegration of high MW cellular and intracellular contents like DNA, proteins and polysaccharides, their release into supernatant, hence increasing the overall fluorescence emission from released compounds and also increasing the MW of

Table 5
Chemical properties of non-treated (sample 0) and treated WAS samples (sample A – no cavitation regime, B – attached cavitation regime, C - developed cloud shedding cavitation regime and D – cavitation in a wake regime).

Sample Parameter	0	A	B	C	D
sCOD (mg L^{-1})	272 ± 0	551 ± 7	735 ± 5	663 ± 3	747 ± 1
NH_4–N (mg L^{-1})	16 ± 0	8 ± 0	30 ± 1	25 ± 0	32 ± 0
NO_3–N (mg L^{-1})	1.4 ± 0.1	1.5 ± 0.3	1.2 ± 0.1	1.1 ± 0.1	1.4 ± 0.1
TSS (g L^{-1})	17.6 ± 0.5	11.4 ± 0.4	8.2 ± 0.0	6.8 ± 0.2	5.1 ± 0.1
DD (%)	–	13.1 ± 0.5	21.7 ± 0.7	18.3 ± 0.6	22.3 ± 0.7
A254	0.52 ± 0.02	1.18 ± 0.02	1.02 ± 0.12	0.86 ± 0.02	0.93 ± 0.05
SUVA	0.66 ± 0.05	0.62 ± 0.09	0.48 ± 0.17	0.45 ± 0.03	0.44 ± 0.05
E465/E665	1.22 ± 0.05	1.59 ± 0.01	1.48 ± 0.01	1.43 ± 0.02	1.47 ± 0.02
Sum A250-450	8512.3 ±866.9	17,267.5 ±244.8	15,567.9 ±3118.9	13,300.7 ±378.6	14,011.6 ±807.7
A260	0.49 ± 0.02	1.14 ± 0.02	0.99 ± 0.16	0.84 ± 0.02	0.91 ± 0.05
A320	0.24 ± 0.02	0.49 ± 0.01	0.43 ± 0.09	0.33 ± 0.01	0.40 ± 0.02
A260/320	2.02 ± 0.11	2.31 ± 0.01	2.30 ± 0.09	2.56 ± 0.03	2.31 ± 0.02

material present in DOM as a result of cavitation. In line with the observed Ex-Em changes in eDOM in response to cavitation, the concomitant effects were deduced at the level of chromogenic DOM as well. The characteristic index E465/E665 and Sum A250-450 showed that all treatments increased MW of DOM in solution (8–33% increase in index values; increased O:C and C:N ratios, increased carboxyl content; reduced aromaticity) and the total amount of chromogenic DOM in solution, respectively. In line with these observations, characterization of nucleic acids utilizing A260, A320 and A260/A320 showed that the amount of DNA as well as chromogenic DOM were increased while their ratio changed in response to cavitation treatments, in line with our recent study (Kolbl-Repinc et al., 2022).

3.4. Evaluation of BMP before and after treatment

A BMP batch test was conducted to evaluate the effects of the selected treatments on methane production. The results of the evolution of cumulative methane production are shown in Fig. 4, with different kinetics observed between samples. Compared to non-treated sample, higher methane production was observed in all treated samples. In the first two days, BMP was high, then came to a halt for about 17 days and continued after day 20. Between the maximum BMPs of all samples the lowest BMP was measured for the non-treated sample on day 37 (183.7 mL CH_4 g^{-1} COD; 127.6 mL CH_4 g^{-1} VS). Between the treated samples sample A had the highest BMP of 312.2 mL CH_4 g^{-1} COD (262.5 mL CH_4 g^{-1} VS) on day 38 followed by samples B, C, and D, where B and C reached the maximum on day 38 (275.6 mL CH_4 g^{-1} COD; 231.7 mL CH_4 g^{-1} VS) and 262.5 mL CH_4 g^{-1} COD; 220.7 mL CH_4 g^{-1} VS, respectively), while D reached the maximum on day 20 (222.5 mL CH_4 g^{-1} COD; 187.1 mL CH_4 g^{-1} VS). Differences in BMP were found between all treated samples, except between samples B and C (Suppl. 5). Furthermore, linear Pearson correlations confirmed the positive or negative correlations between physical/chemical changes (mean particle size *D[4,3]*, mode, d10, d50, d99, sum A250-450, E465/E665) and BMP (Suppl. 3).

The shape of the curve obtained during AD of WAS samples indicates the problems with the anaerobic inoculum (Fig. 4). At this time of the year (summer), the quality of WAS is fluctuating because WWTP also receives the WW from the industry, which could affect the inoculum. Since the inoculum was taken from the anaerobic digester of a WWTP on the day of the experiments (Table 1), this could explain the observed S-shape of the BMP curves (Fig. 4). These inhibitory effects are not related to the experimental procedures as described by (Koch et al., 2019) because there was no modification of inoculum, inoculum to substrate ratio (ISR) on VS basis ISR >2. Therefore, the lag phase can be attributed to the poor microbial activity of the inoculum (Jensen et al., 2011), as the anaerobic digesters of the WWTP were receiving increased flow of industrial WW. The first lag phase, until day 20, observed also for glucose, can be associated with microbial recovery. Thereafter, BMP improved and reached its maximum after 15–20 days. The decrease in BMP observed in samples A and C is because BMP in the blank reactors was higher than in these two reactors.

Studies are available investigating the effects of cavitation on methane production (Lee and Han, 2013; Grübel and Suschka, 2015; Zubrowska-Sudol et al., 2018), (Şağban et al., 2018; Patil et al., 2016), which always report the positive effects of pre-treatment. However, a

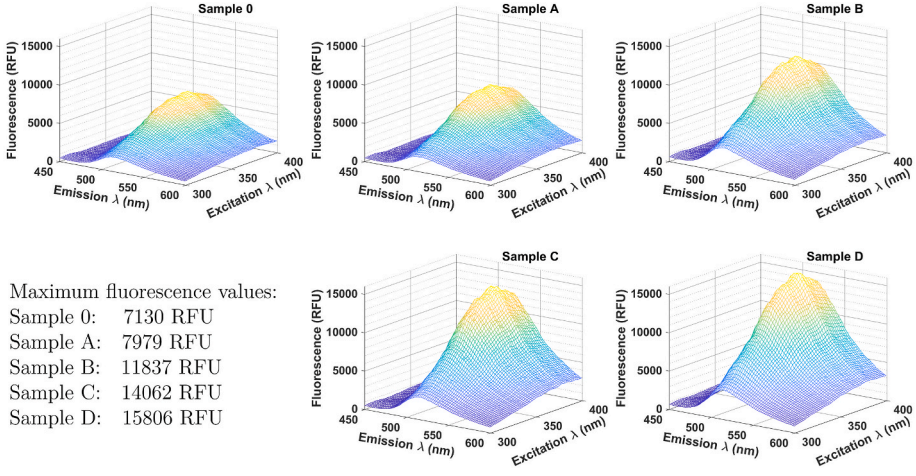

Fig. 3. Examples of Ex-Em spectra before (sample 0) and after treatments (sample A – no cavitation regime, B – attached cavitation regime, C - developed cloud shedding cavitation regime and D – cavitation in a wake regime) with maximum fluorescence values.

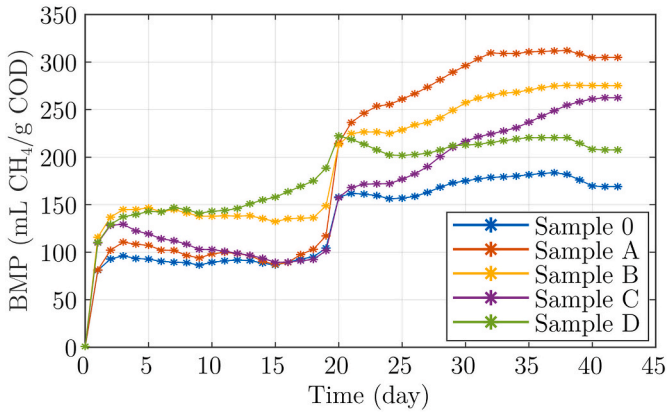

Fig. 4. Biomethane potential for initial sample 0 and all 4 treated samples (sample A – no cavitation regime, B – attached cavitation regime, C – developed cloud shedding regime and D – cavitation in a wake regime). Measurements were performed daily for 42 days.

direct comparison between our and these studies is difficult because there are large differences between the initial WAS samples, the way methane production is given, and the HC devices used. Most of the time it is impossible to determine whether the WAS sample consists only of settled secondary sludge or also primary sludge is included.

It is usually assumed that the physical pre-treatment of WAS increases the degree of solubilization and disintegration, which leads to better biodegradability during AD (Pham et al., 2009) and consequently to higher methane production. However, from the results of this study (Table 5, Figs. 3 and 4), which are consistent with (Zhen et al., 2017), it appears that this is not necessarily the case and that more attention should be paid to the extent to which an increased degree of solubilization and disintegration is important. Our results show that there is no direct correlation between released sCOD, increased fluorescence and methane production and that something else must also be important. We believe that the reason why the highest BMP was obtained in sample A, where the lowest sCOD and fluorescence were determined, might be related to the chemical composition of this sample (see Section 3.3). As mentioned earlier, micro-scale phenomena associated with regimes B, C, and D alter the viscosity and composition of the sample in ways that are not conducive to methane production. This can also be deducted from the pH determined for sample D (8.04 ± 0.31), which was higher than in samples A, B and C (7.86 ± 0.06, 7.89 ± 0.07 and 7.44 ± 0.20, respectively) and could be connected to the chemical composition of samples. This pH is in the upper limit for optimal functioning of the anaerobic archaea (Deublein and Steinhauser, 2010). It seems that it is more important what substances are released from flocs and/or individual cells and what effect a treatment regime has on these substances. Cavitation is known to cause cleavage of synthetic polymer (Petkovšek et al., 2023) and biopolymer chains due to chemical and/or mechanical effects (Holkar et al., 2019), which could also apply to the substances released from flocs and cells in WAS, changing its composition. In addition, due to the chemical effects of cavitation, there may be a varying degree of oxidation of the released compounds, which is not desirable, as discussed in (Neumann et al., 2016). Furthermore, cavitation may also result in the release of active hydrolytic enzymes already present in the EPS and can hence facilitate the subsequent AD process. It must be stressed that, since the general relationship between the chemical composition of the treated WAS and methane production is far from understood, much work is needed to understand its exact role in the AD process. It is important to point out that more detailed chemical analyses of samples in response to cavitation such as size exclusion chromatography, FTIR, NIR and MIR spectroscopy, GS-MS/MS are warranted to map the resulting changes in chemical nature at various levels, as a result of distinct cavitation treatments utilized in this study.

Table 6
Energy balance comparison between four selected treatment regimes (sample A – no cavitation regime, B – attached cavitation regime, C - developed cloud shedding cavitation regime and D – cavitation in a wake regime).

Regime	P_{tre} (kW)	SESS (kJ g^{-1} sCOD)	$CH_4$5L (L)	EE_g (kWh)	EE_r (kWh)	EE_g-EE_r (kWh)
A	0.90	583	6.4	0.064	0.21	−0.141
B	0.70	273	5.0	0.050	0.16	−0.105
C	0.56	258	4.4	0.044	0.12	−0.076
D	0.57	172	1.8	0.018	0.11	−0.095

3.5. Energy balance of treatment

Based on direct energy consumption measurements we were able to determine the energy balance of all 4 treatment regimes. The basic energy calculations, shown in Table 6, indicate that regime C is the most efficient, based on the EE_g-EE_r parameter. Although regime A produced the most additional methane, operational energy consumption diminished its positive impact. It must also be emphasised here that the energy used to increase the static pressure in the system was not considered in the calculations. Additionally, one has to be aware that if the viscosity of the sample is increased, the operating costs of the subsequent AD would increase due to the mixing requirements (Garuti et al., 2018). Comparing the BMP with the physical and chemical properties of all treated samples, it can be concluded that physical properties such as mean particle size and viscosity could be equally important as the chemical properties of WAS such as released sCOD. This implies that pre-treatment methods for WAS should aim to achieve certain physical properties with minimal energy input. Initial step in energy reduction would be to minimize the number of passes while still achieving an appropriate effect on the targeted WAS properties. In the case of the promising treatment regimes (B, C, and D) regarding energy balance, the chemical impact on WAS should be reduced while still increasing methane production.

Even though this study was performed on lab-scale, we are aware that the aspects of energy and economic balance are extremely important if the new technology has any chances to emerge on the market in the future and be used in WWTPs, as already discussed in (Neumann et al., 2016). An additional aspect is a life cycle assessment (Mainardis et al., 2021), which provides even more detailed view on the technology and its overall impact on the environment. Even when considering real scale WAS disintegrators, it is extremely challenging to achieve positive energy and economic balances only from the perspective of additional methane production. Hence, additional beneficial aspects must be considered, such as the shorter retention times of WAS in WWTP's anaerobic digesters, reducing their operational costs. An additional beneficial effect is the overall lower final amount of digested sludge that has to be disposed, usually incinerated, which involves enormous transport and incineration costs.

P_{tre} – power required for treatment; SESS – specific energy of sludge solubilization; $CH_4$5L – potential amount of CH_4 produced by 5L of WAS; EE_g – energy extracted; EE_r – energy required.

4. Conclusions

This study investigated physical methods, based on a rotational cavitation device, for pre-treatment of WAS. We focused on how different types of treatment regimes, one non-cavitating and three cavitating, affect the physical and chemical properties of the WAS samples and ultimately methane production. To exclude cavitation effects and evaluate only shear on macro scale, static pressure was increased in treatment regime A so that no cavitation formed. The other three regimes, B, C, and D were all cavitating and cavitation was varied according to type, magnitude, and intensity by adjusting the rotor-stator

geometry and operating conditions. The main conclusions of the study are as follows:

- All four treatment regimes had statistically significantly different impact on the physical and chemical properties of WAS, stimulating methane production in comparison to non-treated WAS. Micro-scale phenomena due to collapsing cavitation bubbles showed enhanced effects on chemical properties, while shear on macro scale affected the physical properties of WAS more.
- In addition, differences were also found among the three cavitating regimes, indicating that cavitation type has to be carefully chosen for desired effects.
- The change in viscosity could play an important role in methane production, as the highest viscosity increase in the case of treatment regime A resulted in the highest methane production.
- Increased solubilization in the form of sCOD cannot be directly correlated with methane production because the highest sCOD released did not result in the highest BMP.
- Regime with highest BMP did not result in most energy efficient treatment, thus one must strive to achieve optimal energy balance.

Author contributions

M.Z. Conceptualization, investigation, data curation, validation, writing – original draft, review and editing. **B.B.H** Investigation, writing – original draft**. M.D** Formal analysis, writing—review & editing. **J.G.** Investigation, validation, data curation. **M.H.** Formal analysis, writing – review & editing. **L.N.** Formal analysis, writing and review. **S.K.R.** Methodology, writing – original draft.**M.K.** Formal analysis, writing – review & editing. **J.O.** Investigation, visualization, writing – original draft. **Ž.P.** Validation, methodology, writing – original draft. **B.S.** Methodology, validation, writing – original draft. **M.P.** Supervision, data curation, project administration, writing – original draft, review and editing.

Declaration of competing interest

The authors declare that they have no known competing financial interests or personal relationships that could have appeared to influence the work reported in this paper.

Data availability

Data will be made available on request.

Acknowledgements

The authors acknowledge the financial support from the Slovenian Research Agency (research project No. J7-1814, J2-3044, J2-4480, L7-4422, J2-3056, J2-4427, J2-3057, research core funding No. P2-0401, P2-0422, P2-0180), Horizon Europe - 101093964; 101069228 and Horizon 2020 - 771567. Authors would also like to thank the Domžale-Kamnik WWTP for their support.

Appendix B. Supplementary data

Supplementary data to this article can be found online at https://doi.org/10.1016/j.jenvman.2023.119074.

References

APHA, 2005. (2005) Standard Methods for the Examination of Water and Wastewater, twenty-first ed. American Public Health Association/American Water Works Association/Water Environment Federation, Washington DC.

Bhat, A.P., Gogate, P.R., 2021. Cavitation-based pre-Treatment of wastewater and waste sludge for improvement in the performance of biological processes: a review. J. Environ. Chem. Eng. 9, 104743 https://doi.org/10.1016/j.jece.2020.104743.

Cai, M., Hu, J., Lian, G., Xiao, R., Song, Z., Jin, M., Dong, C., Wang, Q., Luo, D., Wei, Z., 2018. Synergetic pretreatment of waste activated sludge by hydrodynamic cavitation combined with Fenton reaction for enhanced dewatering. Ultrason. Sonochem. 42, 609–618. https://doi.org/10.1016/j.ultsonch.2017.11.046.

Carrère, H., Dumas, C., Battimelli, A., Batstone, D.J., Delgenès, J.P., Steyer, J.P., Ferrer, I., 2010. Pretreatment methods to improve sludge anaerobic degradability: a review. J. Hazard Mater. 183, 1–15. https://doi.org/10.1016/j.jhazmat.2010.06.129.

Deublein, D., Steinhauser, A., 2010. Bioreactions. Biogas from waste. Renew. Resour. 101–109 https://doi.org/10.1002/9783527632794.ch10.

Eshtiaghi, N., Markis, F., Yap, S.D., Baudez, J.C., Slatter, P., 2013. Rheological characterisation of municipal sludge: a review. Water Res. 47, 5493–5510. https://doi.org/10.1016/j.watres.2013.07.001.

Fang, W., Zhang, P., Ye, J., Wu, Y., Zhang, H., Liu, J., Zhu, Y., Zeng, G., 2015. Physicochemical properties of sewage sludge disintegrated with high pressure homogenization. Int. Biodeterior. Biodegrad. 102, 126–130. https://doi.org/10.1016/j.ibiod.2015.02.030.

Ferrentino, R., Andreottola, G., 2020. Investigation of sludge solubilization and phosphorous release in anaerobic side-stream reactor with a low pressure swirling jet hydrodynamic cavitation treatment. J. Environ. Chem. Eng. 8, 104389 https://doi.org/10.1016/j.jece.2020.104389.

Garlicka, A., Zubrowska-Sudol, M., 2020. Effect of hydrodynamic disintegration on the solubilisation and bioavailability of thickened excess sludge. Ultrason. Sonochem. 64, 105015 https://doi.org/10.1016/j.ultsonch.2020.105015.

Garuti, M., Langone, M., Fabbri, C., Piccinini, S., 2018. Monitoring of full-scale hydrodynamic cavitation pretreatment in agricultural biogas plant. Bioresour. Technol. 247, 599–609. https://doi.org/10.1016/j.biortech.2017.09.100.

Gherghel, A., Teodosiu, C., De Gisi, S., 2019. A review on wastewater sludge valorisation and its challenges in the context of circular economy. J. Clean. Prod. 228, 244–263. https://doi.org/10.1016/j.jclepro.2019.04.240.

Gonzalez, A., Hendriks, A.T.W.M., van Lier, J.B., de Kreuk, M., 2018. Pre-treatments to enhance the biodegradability of waste activated sludge: elucidating the rate limiting step. Biotechnol. Adv. 36, 1434–1469. https://doi.org/10.1016/j.biotechadv.2018.06.001.

Gostiša, J., Drešar, P., Hočevar, M., Dular, M., 2022. Computational analysis of flow conditions in hydrodynamic cavitation generator for water treatment processes. Can. J. Chem. Eng. 1–15. https://doi.org/10.1002/cjce.24572.

Gostiša, J., Širok, B., Bizjan, B., Ortar, J., Dular, M., Zupanc, M., 2023. Multiparametric experimental analysis of the pin disc rotational cavitation generator. Eng. Sci. Technol. an Int. J. 38 https://doi.org/10.1016/j.jestch.2022.101323.

Gostiša, J., Zupanc, M., Dular, M., Širok, B., Levstek, M., Bizjan, B., 2021. Investigation into cavitational intensity and COD reduction performance of the pinned disc reactor with various rotor-stator arrangements. Ultrason. Sonochem. 77 https://doi.org/10.1016/j.ultsonch.2021.105669.

Grübel, K., Suschka, J., 2015. Hybrid alkali-hydrodynamic disintegration of waste-activated sludge before two-stage anaerobic digestion process. Environ. Sci. Pollut. Res. 22, 7258–7270. https://doi.org/10.1007/s11356-014-3705-y.

Helms, J.R., Stubbins, A., Ritchie, J.D., Minor, E.C., Kieber, D.J., Mopper, K., 2009. Erratum: absorption spectral slopes and slope ratios as indicators of molecular weight, source, and photobleaching of chromophoric dissolved organic matter (Limnology and Oceanography 53 955-969. Limnol. Oceanogr. 54, 1023. https://doi.org/10.4319/lo.2009.54.3.1023.

Holkar, C.R., Jadhav, A.J., Pinjari, D.V., Pandit, A.B., 2019. Cavitationally driven transformations: a technique of process intensification. Ind. Eng. Chem. Res. 58, 5797–5819. https://doi.org/10.1021/acs.iecr.8b04524.

Hong, E., Yeneneh, A.M., Sen, T.K., Ang, H.M., Kayaalp, A., 2018. A comprehensive review on rheological studies of sludge from various sections of municipal wastewater treatment plants for enhancement of process performance. Adv. Colloid Interface Sci. 257, 19–30. https://doi.org/10.1016/j.cis.2018.06.002.

Hou, R., Song, Y., Liu, J., Zhang, L., Zhang, M., Sun, X., 2023. Experimental and numerical investigation on the disinfection characteristics of a novel rotor-radial groove hydrodynamic cavitation reactor. Process Saf. Environ. Protect. 169, 260–269. https://doi.org/10.1016/j.psep.2022.11.019.

Jensen, P.D., Ge, H., Batstone, D.J., 2011. Assessing the role of biochemical methane potential tests in determining anaerobic degradability rate and extent. Water Sci. Technol. 64, 880–886. https://doi.org/10.2166/wst.2011.662.

Jpm learning library [WWW Document], n.d. URL https://www.jmp.com/en_ch/learning-library/topics/basic-inference–proportions-and-means.html (accessed 3.10.23).

Khanh Nguyen, V., Kumar Chaudhary, D., Hari Dahal, R., Hoang Trinh, N., Kim, J., Chang, S.W., Hong, Y., Duc La, D., Nguyen, X.C., Hao Ngo, H., Chung, W.J., Nguyen, D.D., 2021. Review on pretreatment techniques to improve anaerobic digestion of sewage sludge. Fuel 285, 119105. https://doi.org/10.1016/j.fuel.2020.119105.

Kim, H., Koo, B., Sun, X., Yoon, J.Y., 2020. Investigation of sludge disintegration using rotor-stator type hydrodynamic cavitation reactor. Sep. Purif. Technol. 240, 116636 https://doi.org/10.1016/j.seppur.2020.116636.

Kim, H., Sun, X., Koo, B., Yoon, J.Y., 2019. Experimental investigation of sludge treatment using a rotor-stator type hydrodynamic cavitation reactor and an ultrasonic bath. Processes 7. https://doi.org/10.3390/pr7110790.

Kim, H.J., Nguyen, D.X., Bae, J.H., 2008. The performance of the sludge pretreatment system with venturi tubes. Water Sci. Technol. 57, 131–137. https://doi.org/10.2166/wst.2008.717.

Koch, K., Hafner, S.D., Weinrich, S., Astals, S., 2019. Identification of critical problems in biochemical methane potential (BMP) tests from methane production curves. Front. Environ. Sci. 7, 1–8. https://doi.org/10.3389/fenvs.2019.00178.

Kolbl-Repinc, S., Bizjan, B., Budhiraja, V., Dular, M., Gostiša, J., Brajer Humar, B., Kaurin, A., Kržan, A., Levstek, M., Arteaga, J.F.M., Petkovšek, M., Rak, G., Stres, B., Širok, B., Žagar, E., Zupanc, M., 2022. Integral analysis of hydrodynamic cavitation effects on waste activated sludge characteristics, potentially toxic metals, microorganisms and identification of microplastics. Sci. Total Environ. 806 https://doi.org/10.1016/j.scitotenv.2021.151414.

Kolbl, S., Forte-Tavčer, P., Stres, B., 2017. Potential for valorization of dehydrated paper pulp sludge for biogas production: addition of selected hydrolytic enzymes in semi-continuous anaerobic digestion assays. Energy 126, 326–334. https://doi.org/10.1016/j.energy.2017.03.050.

Kolbl, S., Paloczi, A., Panjan, J., Stres, B., 2014. Addressing case specific biogas plant tasks: industry oriented methane yields derived from 5L Automatic Methane Potential Test Systems in batch or semi-continuous tests using realistic inocula, substrate particle sizes and organic loading. Bioresour. Technol. 153, 180–188. https://doi.org/10.1016/j.biortech.2013.12.010.

Lee, G., Lee, I., Han, J.I., 2019. A combined method of hydrodynamic cavitation and alkaline treatment for waste-activated sludge solubilization; N/P recovery from anaerobic granular sludge. J. Environ. Chem. Eng. 7, 103329 https://doi.org/10.1016/j.jece.2019.103329.

Lee, I., Han, J.I., 2013. The effects of waste-activated sludge pretreatment using hydrodynamic cavitation for methane production. Ultrason. Sonochem. 20, 1450–1455. https://doi.org/10.1016/j.ultsonch.2013.03.006.

Mainardis, M., Buttazzoni, M., Gievers, F., Vance, C., Magnolo, F., Murphy, F., Goi, D., 2021. Life cycle assessment of sewage sludge pretreatment for biogas production: from laboratory tests to full-scale applicability. J. Clean. Prod. 322, 129056 https://doi.org/10.1016/j.jclepro.2021.129056.

Mancuso, G., 2018. Experimental and numerical investigation on performance of a swirling jet reactor. Ultrason. Sonochem. 49, 241–248. https://doi.org/10.1016/j.ultsonch.2018.08.011.

Mancuso, G., Langone, M., Andreottola, G., 2017. A swirling jet-induced cavitation to increase activated sludge solubilisation and aerobic sludge biodegradability. Ultrason. Sonochem. 35, 489–501. https://doi.org/10.1016/j.ultsonch.2016.11.006.

Mancuso, G., Langone, M., Andreottola, G., Bruni, L., 2019. Effects of hydrodynamic cavitation, low-level thermal and low-level alkaline pre-treatments on sludge solubilisation. Ultrason. Sonochem. 59 https://doi.org/10.1016/j.ultsonch.2019.104750.

Mancuso, G., Langone, M., Di Maggio, R., Toscano, A., Andreottola, G., 2021. Effect of hydrodynamic cavitation on flocs structure in sewage sludge to increase stabilization for efficient and safe reuse in agriculture. Ann. Finance 26, 41–52. https://doi.org/10.1080/10889868.2021.1900055.

Nabi, M., Zhang, G., Zhang, P., Tao, X., Wang, S., Ye, J., Zhang, Q., Zubair, M., Bao, S., Wu, Y., 2019. Contribution of solid and liquid fractions of sewage sludge pretreated by high pressure homogenization to biogas production. Bioresour. Technol. 286, 121378 https://doi.org/10.1016/j.biortech.2019.121378.

Neumann, P., Pesante, S., Venegas, M., Vidal, G., 2016. Developments in pre-treatment methods to improve anaerobic digestion of sewage sludge. Rev. Environ. Sci. Biotechnol. 15, 173–211. https://doi.org/10.1007/s11157-016-9396-8.

Parandoush, S., Mokhtarani, N., 2022. Reducing excess sludge volume in sequencing batch reactor by integrating ultrasonic waves and ozonation. J. Environ. Manag. 317, 115405 https://doi.org/10.1016/j.jenvman.2022.115405.

Patil, P.N., Gogate, P.R., Csoka, L., Dregelyi-Kiss, A., Horvath, M., 2016. Intensification of biogas production using pretreatment based on hydrodynamic cavitation. Ultrason. Sonochem. 30, 79–86. https://doi.org/10.1016/j.ultsonch.2015.11.009.

Petkovšek, M., Kržan, A., Šmid, A., Žagar, E., Zupanc, M., 2023. Degradation of water soluble poly(vinyl alcohol) with acoustic and hydrodynamic cavitation: laying foundations for microplastics. npj Clean Water 6, 1–11. https://doi.org/10.1038/s41545-023-00248-8.

Petkovšek, M., Mlakar, M., Levstek, M., Stražar, M., Širok, B., Dular, M., 2015. A novel rotation generator of hydrodynamic cavitation for waste-activated sludge disintegration. Ultrason. Sonochem. 26, 408–414. https://doi.org/10.1016/j.ultsonch.2015.01.006.

Pham, T.T.H., Brar, S.K., Tyagi, R.D., Surampalli, R.Y., 2009. Ultrasonication of wastewater sludge-Consequences on biodegradability and flowability. J. Hazard Mater. 163, 891–898. https://doi.org/10.1016/j.jhazmat.2008.07.091.

Pilli, S., Bhunia, P., Yan, S., LeBlanc, R.J., Tyagi, R.D., Surampalli, R.Y., 2011. Ultrasonic pretreatment of sludge: a review. Ultrason. Sonochem. 18, 1–18. https://doi.org/10.1016/j.ultsonch.2010.02.014.

PROMEGA Application Note [WWW Document], n.d. URL https://worldwide.promega.com/resources/pubhub/enotes/how-do-i-determine-the-concentration-yield-and-purity-of-a-dna-sample/(accessed 11.17.22, page 1).

Rajasulochana, P., Preethy, V., 2016. Comparison on efficiency of various techniques in treatment of waste and sewage water – a comprehensive review. Resour. Technol. 2, 175–184. https://doi.org/10.1016/j.reffit.2016.09.004.

Ruiz-Hernando, M., Simón, F.X., Labanda, J., Llorens, J., 2014. Effect of ultrasound, thermal and alkali treatments on the rheological profile and water distribution of waste activated sludge. Chem. Eng. J. 255, 14–22. https://doi.org/10.1016/j.cej.2014.06.036.

Ruiz-Hernando, M., Vinardell, S., Labanda, J., Llorens, J., 2022. Effect of ultrasonication on waste activated sludge rheological properties and process economics. Water Res. 208, 117855 https://doi.org/10.1016/j.watres.2021.117855.

Şağban, F.O.T., Dindar, E., Cirakoglu, C., Keskinler, B., 2018. Hydrodynamic cavitation of waste-activated sludge. Environ. Eng. Sci. 35, 775–784. https://doi.org/10.1089/ees.2016.0408.

Stepišnik Perdih, T., Širok, B., Dular, M., 2017. Influence of hydrodynamic cavitation on intensification of laundry aqueous detergent solution preparation. J. Mech. Eng. 63, 83–91. https://doi.org/10.5545/sv-jme.2016.3970.

Twardowski, M.S., Boss, E., Sullivan, J.M., Donaghay, P.L., 2004. Modeling the spectral shape of absorption by chromophoric dissolved organic matter. Mar. Chem. 89, 69–88. https://doi.org/10.1016/j.marchem.2004.02.008.

Vilarroig, J., Martínez, R., Zuriaga-Agustí, E., Torró, S., Galián, M., Chiva, S., 2020. Design and optimization of a semi-industrial cavitation device for a pretreatment of an anaerobic digestion treatment of excess sludge and pig slurry. Water Environ. Res. 92, 2060–2071. https://doi.org/10.1002/wer.1366.

Wang, B., Su, H., Zhang, B., 2021. Hydrodynamic cavitation as a promising route for wastewater treatment – a review. Chem. Eng. J. 412, 128685 https://doi.org/10.1016/j.cej.2021.128685.

Wang, X., Jiang, C., Wang, H., Xu, S., Zhuang, X., 2023. Strategies for energy conversion from sludge to methane through pretreatment coupled anaerobic digestion: potential energy loss or gain. J. Environ. Manag. 330, 117033 https://doi.org/10.1016/j.jenvman.2022.117033.

Xu, Y., Lu, Y., Zheng, L., Wang, Z., Dai, X., 2020. Perspective on enhancing the anaerobic digestion of waste activated sludge. J. Hazard Mater. 389, 121847 https://doi.org/10.1016/j.jhazmat.2019.121847.

Yao, Y., Sun, Y., Wang, X., Song, Y., Wang, Z., 2022. Insight into the sludge reduction performances by hydrodynamic cavitation. J. Water Process Eng. 49, 102950 https://doi.org/10.1016/j.jwpe.2022.102950.

Zhang, J., Xu, S., Li, W., 2012. High shear mixers: a review of typical applications and studies on power draw, flow pattern, energy dissipation and transfer properties. Chem. Eng. Process. Process Intensif. 57 (58), 25–41. https://doi.org/10.1016/j.cep.2012.04.004.

Zhang, S., Liang, J., Huang, J., Huang, S., Zheng, L., Sun, S., Zhong, Z., Zhang, X., Yu, X., Guan, Z., 2019. Analysis of the relationship of extracellular polymeric substances to the dewaterability and rheological properties of sludge treated by acidification and anaerobic mesophilic digestion. J. Hazard Mater. 369, 31–39. https://doi.org/10.1016/j.jhazmat.2019.02.012.

Zhen, G., Lu, X., Kato, H., Zhao, Y., Li, Y.Y., 2017. Overview of pretreatment strategies for enhancing sewage sludge disintegration and subsequent anaerobic digestion: current advances, full-scale application and future perspectives. Renew. Sustain. Energy Rev. 69, 559–577. https://doi.org/10.1016/j.rser.2016.11.187.

Zubrowska-Sudol, M., Dzido, A., Garlicka, A., Krawczyk, P., Stępien, M., Umiejewska, K., Walczak, J., Wołowicz, M., Sytek-Szmeichel, K., 2020. Innovative hydrodynamic disintegrator adjusted to agricultural substrates pre-treatment aimed at methane production intensification—cfd modelling and batch tests. Energies 13. https://doi.org/10.3390/en13164256.

Zubrowska-Sudol, M., Podedworna, J., Sytek-Szmeichel, K., Bisak, A., Krawczyk, P., Garlicka, A., 2018. The effects of mechanical sludge disintegration to enhance full-scale anaerobic digestion of municipal sludge. Therm. Sci. Eng. Prog. 5, 289–295. https://doi.org/10.1016/j.tsep.2017.11.009.

Zupanc, M., Pandur, Ž., Stepišnik Perdih, T., Stopar, D., Petkovšek, M., Dular, M., 2019. Effects of cavitation on different microorganisms: the current understanding of the mechanisms taking place behind the phenomenon. A review and proposals for further research. Ultrason. Sonochem. 57, 147–165. https://doi.org/10.1016/j.ultsonch.2019.05.009.